Visualization of advanced human prostate cancer lesions in living mice by a targeted gene transfer vector and optical imaging

Jason Y. Adams,[1] Mai Johnson,[1] Makoto Sato,[1] Frank Berger,[2] Sanjiv S. Gambhir,[2] Michael Carey[3], M. Luisa Iruela-Arispe[4] & Lily Wu[1]

Departments of [1]Urology and [2]Crump Institute for Molecular Imaging & Department of Molecular & Medical Pharmacology, [3]Biological Chemistry, David Geffen School of Medicine at UCLA, and [4]Department of Molecular Cell and Developmental Biology, College of Letters & Science, UCLA, Los Angeles California 90095, USA

Correspondence should be addressed to L.W.; email: lwu@mednet.ucla.edu

Non-invasive imaging and transcriptional targeting can improve the safety of therapeutic approaches in cancer. Here we demonstrate the ability to identify metastases in a human-prostate cancer model, employing a prostate-specific adenovirus vector (AdPSE-BC-luc) and a charge-coupled device-imaging system. AdPSE-BC-luc, which expresses firefly luciferase from an enhanced prostate-specific antigen promoter, restricted expression in the liver but produced robust signals in prostate tumors. In fact, expression was higher in advanced, androgen-independent tumors than in androgen-dependent lesions. Repetitive imaging over a three-week period after AdPSE-BC-luc injection into tumor-bearing mice revealed that the virus could locate and illuminate metastases in the lung and spine. Systemic injection of low doses of AdPSE-BC-luc illuminated lung metastasis. These results demonstrate the potential use of a non-invasive imaging modality in therapeutic and diagnostic strategies to manage prostate cancer.

Improvements in screening and treatment of localized disease have led to a steady decline in prostate cancer mortality over the past 10 years[1]. Despite these advancements, prostate cancer is the second leading cause of cancer deaths in American men. Endocrine therapy, using androgen ablation, is the current treatment for advanced, metastatic disease[2]. However, the disease invariably relapses within 18–36 months[3], after which it is considered androgen independent (AI) with no effective treatment. Vector-based gene therapy represents a potential alternative or adjuvant to existing therapies for the treatment of AI disease[4]. Strong constitutive viral promoters, such as cytomegalovirus (CMV), enable high transgene expression, but these are not specific. To improve the activity and specificity of prostate-targeted gene expression, we developed enhanced promoters by multimerizing key regulatory elements in the prostate-specific antigen (PSA) enhancer and promoter[5]. The PSE-BC construct was 20-fold more active than the native PSA enhancer/promoter. Furthermore, when incorporated into an adenovirus vector (AdPSE-BC-luc), the promoter exhibited enhanced prostate specificity and restricted expression[5].

To advance the concept of prostate-targeted expression, we tested our approaches in several human prostate cancer (CaP) xenograft models (LAPC series), in severe combined immune-deficient (SCID) mice. The models retain characteristics of clinical disease, including androgen receptor (AR) and PSA

expression, androgen requirement, and metastatic potential[6,7]. Demonstration of the utility of our approaches in relevant models suggests that they may be applicable in clinical settings.

The cooled charged-coupled device (CCD) camera is a sensitive optical imaging system for detecting bioluminescence emitted from D-luciferin reacting with firefly luciferase in living animals[8,9]. The advantages of a targeted gene transfer approach coupled with non-invasive imaging include the ability to localize diseased tissue, and importantly, to accurately monitor the kinetics and levels of transgene expression *in vivo*. Here we employed CCD imaging to achieve those ends in mouse models of human CaP.

Calibration of optical CCD signals

Optical CCD imaging has been applied to study animal models of cancer marked with a luciferase gene[8]. The imaging signals generated by a tissue-specific, vector-based approach are not well documented. The CCD signals, which are specifically dependent on the administration of D-luciferin substrate, were quantified as maximum relative light units per minute of acquisition time (RLU/min). To estimate the sensitivity, 1×10^4 to 1×10^6 LNCaP prostate cancer cells, infected with AdCMV-luc or AdPSE-BC-luc, were implanted into the peritoneum. Light signals emitted by 1×10^4, 1×10^5 and 1×10^6 AdCMV-luc-infected cells were 1.4×10^3, 2.3×10^4 and 2.0×10^5 RLU/min, respectively. In comparison, 1×10^5 and 1×10^6 AdPSE-BC-luc-infected cells produced 170 and 1,800 RLU/min, respectively.

Discriminatory expression capability of AdPSE-BC-luc

We assessed the *in vivo* transcriptional targeting capability of AdPSE-BC-luc in comparison to AdCMV-luc[9]. After tail-vein injection of the virus, firefly luciferase expression was monitored by CCD imaging. Despite comparable gene delivery in both groups (Fig. 1*b*), AdPSE-BC-luc-mediated expression in the liver was less than 1×10^{-5} that of AdCMV-luc (Fig. 1*a*). The direct prostate-specific transcriptional activity of AdPSE-BC-luc was evaluated by injection into human CaP tumors. The results from androgen-dependent (AD) LAPC-4 models are shown in Fig. 2*b*. Similar results were observed in LAPC-9 tumors (data not shown). At 11 days post-injection, the average signal in the AdPSE-BC-luc cohort ($n = 5$, 1.3×10^3) displayed a 32-fold lower activity than the AdCMV-luc cohort ($n = 3$, 4.2×10^4). By comparing the ratio of activity in LAPC-4 tumors with that in liver,
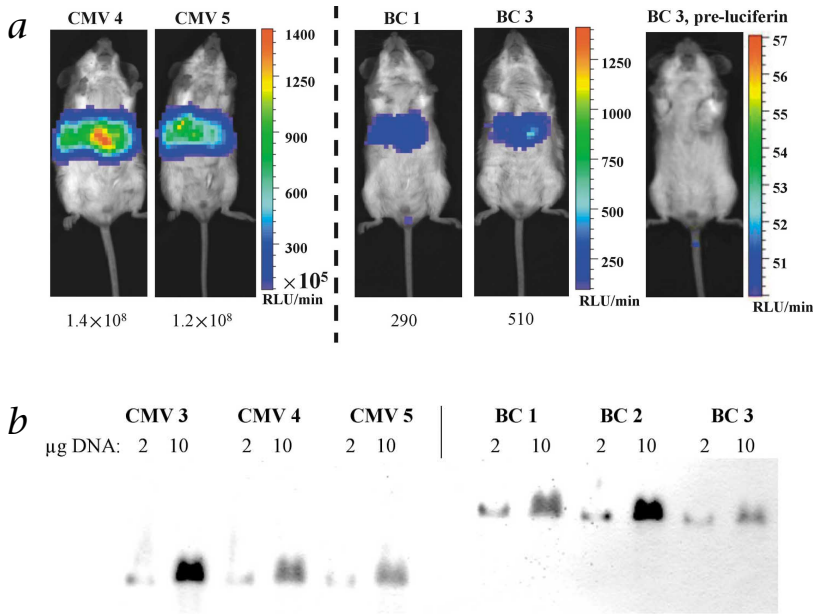
Fig. 1 Adenoviral vector-mediated luciferase gene delivery and expression in the liver after systemic administration. *a*, CCD images of mice injected with either AdCMV-luc or the prostate-specific AdPSE-BC-luc via tail vein. The images represent the results from 2 animals of each cohort at 4 d post-injection. The animal designation is indicated above the images. BC1 and BC3 represent mice #1 and #3, respectively, in the AdPSE-BC-luc group, and CMV4 and CMV5 indicate the AdCMV-luc-injected animals. The relative light intensity (RLU/min) emitted from the animal was quantified by image analysis software and represented by the color scale, shown next to the images. The maximal signal intensity (maximum RLU/min) is shown below each image. The acquisition times were reduced to offset saturated liver signal intensities in AdCMV-luc cohort. *b*, Adenoviral gene transfer in livers of two cohorts injected either with AdCMV-luc or AdPSE-BC-luc. Southern-blot analysis of total cellular DNA was shown. *Not*I restriction liberated a 2.8-kb CMV-luc and a 4.6-kb PSE-BC-luc expression cassette. DNA (2 μg and 10 μg) of each sample was analyzed.

AdPSE-BC-luc exhibited ~3,000-fold higher specific expression in CaP tumors than AdCMV-luc (Figs. 1 and 2). Systemic administration of AdPSE-BC-luc resulted in the highest luciferase expression in mouse prostates and LAPC-9 tumors[5]. These results suggest that AdPSE-BC-luc exhibits exquisite prostate-specificity and is able to restrict expression in non-prostate organs (such as liver).

Kinetics of transgene expression in living mice

One major advantage of the CCD non-invasive imaging system is the ability for repetitive monitoring of luciferase gene expression in the same animal over time. Over a 3-week period, the AdCMV-luc-injected mouse (CMV1) displayed high intratumoral signals 2–4 days post-injection (Fig. 2a). Leakage of AdCMV-luc into the circulation after intratumoral injections was indicated by the signals appearing in the liver (Fig. 2a). In

fact, after 4 days, the liver signals exceeded those in the tumor, and remained at $~1.5 \times 10^6$ RLU/min (Fig. 2a). The intratumoral signals gradually decrease to below 4×10^4 RLU/min, the minimum scale set for this experiment.

The time-course of intratumoral AdPSE-BC-luc expression was delayed (Fig. 2), which may be attributed to its lower intrinsic activity relative to Ad-CMV-luc. AdPSE-BC-luc-injected tumors expressed negligible luciferase at two days post-injection (3 of 5 mice) (data not shown). Signals were apparent at 4 days, and peaked 8–11 days post-injection (Fig. 2b). In the AdPSE-BC-luc-injected cohort, only signals emitted from the tumors were detected on or before 11 days post-injection (Fig. 2b). However, at 21 days post-injection, low-magnitude extratumoral signals were visible (~200 RLU/min) (Fig. 2b) emanating from the lower back and chest. These signals were above the background luminescence of less than 70 RLU/min.
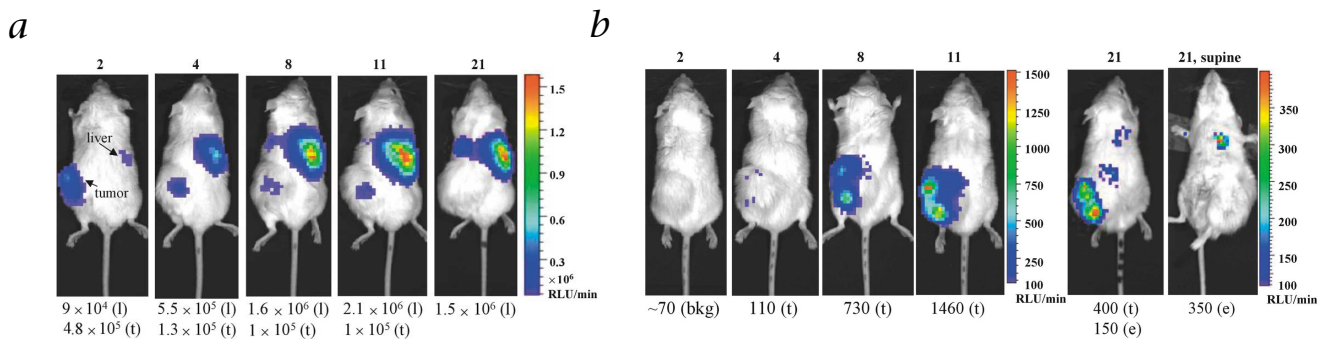

Fig. 2 Kinetics of transgene expression in living mice after intratumoral injection. *a*, Location and magnitude of luciferase expression in an AdCMV-luc-injected mouse (CMV1). Images from sequential d after injection (indicated at the top of each image) displayed two sites of optical signal, that is, in the liver (l) and in the tumor (t). Tumor signal at 21 d post-injection was below 4×10^4. 1.8×10^9 infectious units of Ad were injected into ~7-mm diameter tumors in six divided doses in two consecutive d. In the AdCMV-luc-injected cohort of 3 mice, the average signal (RLU/min) in the tumor was 7.2×10^4, 4.3×10^4, 4.2×10^4, respectively, on day 4, 8, 11. The liver signal on the same time points was 3.3×10^5, 1.1×10^6, 1.0×10^6, respectively. *b*, Luciferase-expression profile of an AdPSE-BC-luc-injected animal (BC4). The signals in the tumor (t) and extratumoral lesions (e) are specified below the images. The background luminescence signal at 2 d post-infection was ≤ 70 RLU/min. In the AdPSE-BC-luc-injected cohort of 5 mice, the average signal in the tumor was 900, 1,800 and 1,300, respectively, on days 4, 8 and 11. Low-magnitude extratumoral signals (~200 RLU/min) were visible in the chest and or back (3 of 5 mice).
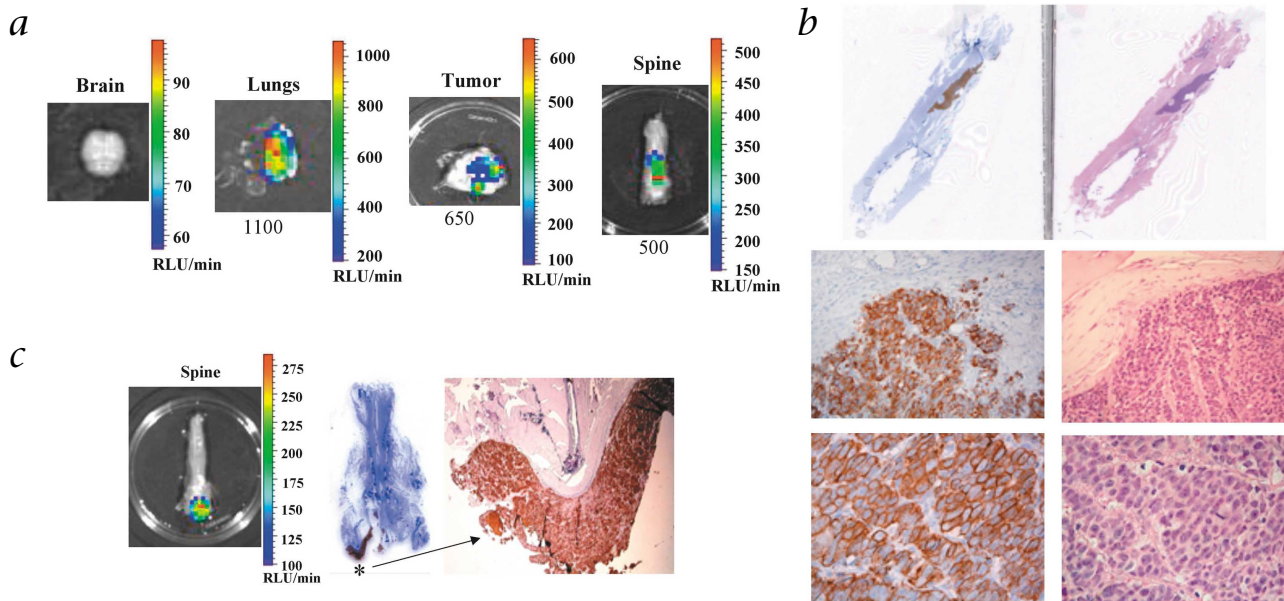
a

b

c

Fig. 3 Detailed histological analysis of spinal metastatic lesions. *a*, The isolated organs from mouse BC4 (Fig. 2*b*) were imaged. Due to light signal attenuation contributed by the covering tissues, the isolated organs displayed higher signal intensities than in the intact living animal[9]. *b*, Histological analysis of the spine lesion of mouse BC4. 5-μm sections of spine were stained with H&E (right) and with human-specific antibody against cytokeratin (left). Unmagnified sections (top) show an elongated lesion in the mid-segment of the spine. Higher magnifications (×200, middle and ×400, bottom) of the lesion are shown. Anti-human cytokeratin specifically stained the lesion with a characteristic intense ring of cytoplasmic staining. *c*, Correspondence of CCD signal and location of a spinal lesion. In another mouse, BC2, with spinal signal, anti-human cytokeratin stain localized the lesion to the caudal end of the spine. Magnification, ×40 in right panel.

Detection and localization of metastases

To localize the origin of the extratumoral luminescence, we isolated organs from the (BC4) mouse and re-imaged them (Fig. 3*a*). The signals in the chest and lower back were found to originate from the lung and spine, respectively (Figs. 2*b* and 3). Histological analysis of the spinal column revealed a lesion localized to the mid-segment (Fig. 3*a* and *b*). Higher magnifications revealed an elongated lesion embedded in spinal musculature, characterized by large pleomorphic nuclei and a high mitotic rate consistent with neoplasia (Fig. 3*b*). Human cytokeratin staining confirmed the lesion was of human origin (Fig. 3*b*). The spinal lesion from another animal (BC2) had the same histological characteristics and a clear correspondence of CCD signal to the lesion located at the caudal end of the spine (Fig. 3*c*).

Immunofluorescent confocal microscopy was used to identify metastatic lung lesions. The lungs of non-tumor-bearing mice stained negative for human cytokeratin (data not shown). Microscopic evaluation of lung sections from tumor-bearing mice revealed the characteristic cytoplasmic cytokeratin staining (Fig. 4*a*). Tumor cells were detected as micrometastatic nodules of 9–74 cells in several independent locations that occupied 377 μm³ of the right lung and 46 μm³ of the left lung. The predominant localization of micrometastasis in the right lung corresponded well with the CCD imaging (Fig. 4*a*).
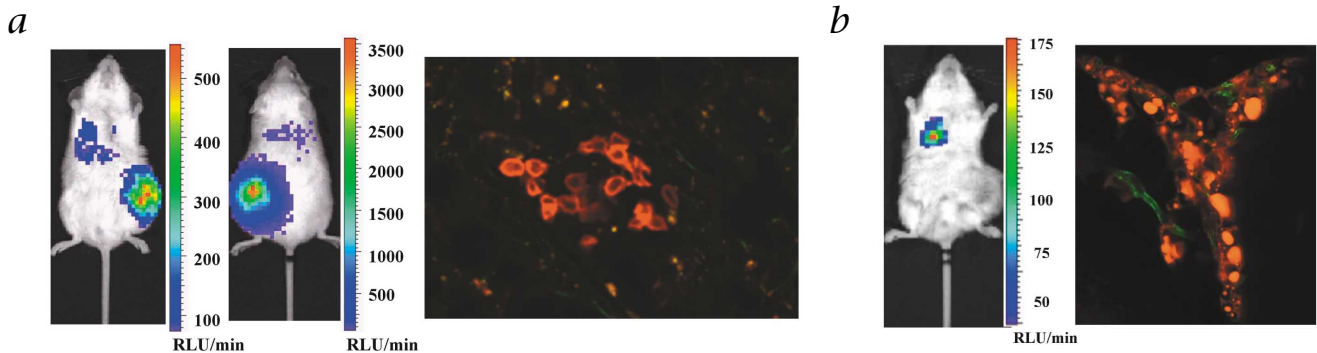
a

b

Fig. 4 Optical CCD detection and histological analysis of lung metastases. *a*, Detection of lung metastasis by CCD imaging and confocal microscopy. In the mouse images, upper chest signals were greater in right image, and were detected in a LAPC-4 AI tumor-bearing mouse (BC1) 21 d after intratumoral injection of 1.8×10^9 infectious units of AdPSE-BC-luc. The right panel is a representative confocal microscopic image of metastatic cells in the lung. On the far right, the cluster of cells exhibits the positive staining of anti-cytokeratin. Magnification, ×400. *b*, Detection of lung metastases after systemic injection of AdPSE-BC-luc. 3.6 $\times 10^7$ infectious units were injected via the tail vein in a LAPC-4 AD tumor-bearing mouse. Left panel shows the image at 12 d after injection. Right panel shows a lung section stained positive using anti-cytokeratin (red/orange) visualized in confocal microscopy. Magnification, ×400. Vessels were visualized by lectin (green).

To our knowledge, detection of metastases by a vector-based imaging approach in living animals has not yet been reported. Thus, we investigated whether systemic vector delivery could visualize metastasis. Two expected challenges of systemic delivery are, first, that most of the adenovirus will likely be sequestered in the liver[10], resulting in greatly reduced delivery to organs in the arterial circulation[5]; and second, that systemic delivery of high doses of adenovirus can result in liver toxicity and immune activation[11]. Due to these issues, we focused on determining the lowest viral dose that would allow us to detect metastases. We administered 1.8×10^7 and 3.6×10^7 infectious units of AdPSE-BC-luc (50- to 100-fold lower than the intratumoral injection dose). No specific signals were detected using the lowest dose (data not shown). However, lung metastasis was visualized 12 days after tail-vein injection of the 3.6×10^7 plaque-forming units (p.f.u.) (Fig. 4b). Confocal microscopy confirmed the presence of metastatic cancer cells (Fig. 4b).

Elevated PSA-based expression in AI tumors

One of the challenges facing the prostate cancer field is localization of recurrent AI disease. We first compared endogenous AR and PSA expression in AD and AI tumors. PSA and AR protein expression increased in the AI subline (Fig. 5a). AdPSE-BC-luc-mediated luciferase expression paralleled the endogenous PSA increase (Fig. 5b). The CCD images of two mice from AD and AI LAPC-4 tumor-bearing cohorts are shown (Fig. 5b). The averaged signal in AI was 10-fold higher than that in the AD cohort 11 days post-injection ($n = 4$). Uneven vector distribution and gene transfer are limitations of intratumoral injec-tions. To rule out these possibilities, we performed *ex vivo* infection of single-cell suspensions derived from the AD and AI xenografts. Both tumor cells were equally infected (data not shown). Luciferase expression 3 days after AdPSE-BC infection was $5.80 \pm 0.87 \times 10^4$ RLU/μg protein in AI LAPC-4 as compared with $2.37 \pm 0.79 \times 10^4$ RLU/μg protein in AD tumor cells ($P = 0.007$, two-tailed *t*-test).

Luciferase expression regulated by the PSA-derived PSE-BC promoter seemed to correlate to the endogenous PSA level, but not to tumor volume (Fig. 5a and b). To investigate this issue further, we infected LNCaP cells, an androgen-responsive prostate cancer line, with AdPSE-BC-luc. We determined the luciferase activity (Fig. 5c) and endogenous PSA and AR expression (Fig. 5c) with varying concentrations of synthetic androgen, R1881, added to culture media. Luciferase expression in LNCaP cells mediated by AdPSE-BC-luc exhibited strong androgen inducibility and correlation to endogenous PSA and AR but not to ubiquitous cellular proteins (that is, actin).

Discussion

Hormone therapy for prostate cancer has changed little since its introduction 30 years ago. As a result, gene-based therapeutic strategies, covering a broad spectrum of approaches including replacement of defective tumor suppressors, cytotoxic enzyme-prodrug therapy, suppression of tumor angiogenesis, and up-regulation of immune-mediated tumor surveillance[4], have emerged as promising alternatives or adjuvants to existing modalities. However, the design and application of vector-based cancer gene therapies must address both efficacy and safety.
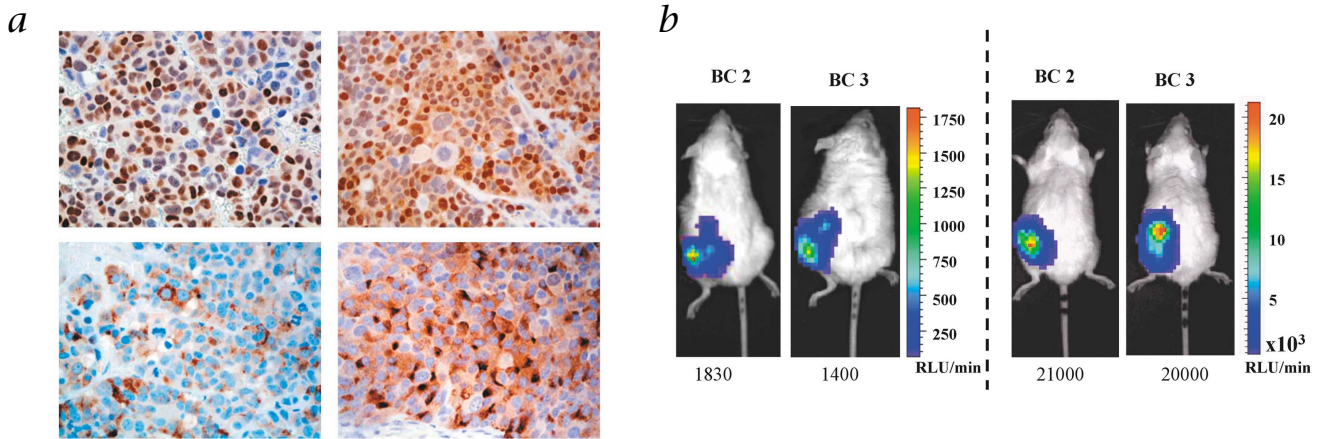

a

b

c

Fig. 5 Androgen-regulated gene expression in prostate cancer models. *a*, Endogenous AR (top) and PSA (bottom) expression in AD (left) and AI (right) LAPC-4 tumors. Brown staining indicates positive expression. PSA expression in the AI tumor appears to be elevated compared with the AD LAPC-4 tumor. AR expression appears less well localized to the nucleus in the AI tumor. *b*, CCD images of LAPC-4 AD (left) or AI (right) tumor-bearing mice 11 d after intratumoral injection. Representative animals from each cohort are shown. The average signal of 4 AI tumor-bearing mice at day 8 and 11 is 8,600 and 13,000 RLU/min, respectively. *c*, Androgen regulated expression in LNCaP cells mediated by AdPSE-BC-luc. Before infection, LNCaP cells were cultured in 0 androgen media for 24 h. After infection, specified concentration of R1881 or Casodex (anti-androgen) was added. The graph denotes the average of triplicated experiment of luciferase expression 48 h after infection with standard error bar (top). The expression in 0 R1881, 1 and 10 μm Casodex were 280, 190 and 260, respectively. An aliquot of cells treated under the same conditions was collected for western-blot analysis (bottom). Equal aliquot of cells containing ~10 μg of total protein was loaded in each lane. The β-actin expression served as internal control.
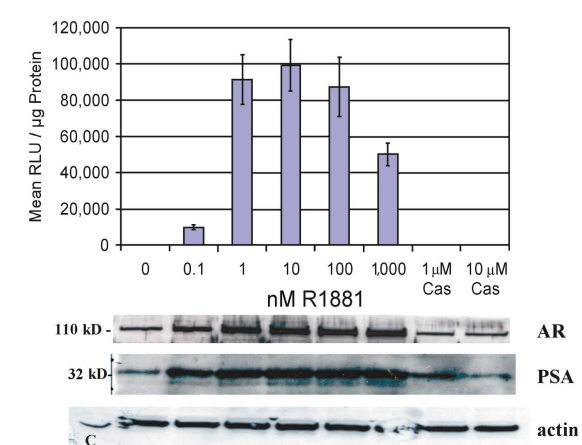
Methods

Mice and LAPC xenograft propagation and cell cultures. Approximately 1×10^6 LAPC-4 seed tumor cells generously provided by C. Sawyers[6,7], were mixed 1:1 with Matrigel (Collaborative Research, Bedford, Massachusetts) and implanted subcutaneously in male SCID (scid/scid) mice. The AI sublines were passaged several rounds in castrated male mice[6]. Single-cell suspension cultures of xenografts[7] were maintained on PreBM/GM media (Clonetics, Walkersville Maryland). LNCaP cells were maintained in RPMI media (Invitrogen, Carlsbad, California) with 10% FBS. In 0 androgen condition, 10% charcoal-treated FBS (ref. 5) was used. Methylenetrienolone (R1881; NEN Life Science Products, Boston, Massachusetts) was added at specified concentration.

Adenoviral vectors, Southern hybridization and immunoblotting. AdCMV-luc and AdPSE-BC-luc[5,9] were titered by plaque assays on 293 monolayer cells (infectious units = plaque-forming units). Total DNA was purified by phenol/chloroform extraction and ethanol precipitation after the liver tissues were homogenized and lysed by proteinase K. Southern hybridization conditions are as previously described[5]. Non-radioactive digoxigenin (Roche Molecular Biochemicals, Mannheim, Germany) labeled luciferase DNA fragment was used as probe[5].

LNCaP cells were infected at 10 infectious units/cell, harvested and lysed using RIPA lysis buffer (10 mM Tris, 150 mM NaCl, 0.1% SDS, 1% DOC, 1 mM EDTA and 1% NP40) and 10 µg of protein per lane were analyzed. Primary antibody to PSA (Dako, Copenhagen, Denmark), AR (Upstate, Lake Placid, New York) and actin (Sigma, St. Louis, Missouri) were used. Specific protein was visualized by ECL (Amersham, Piscataway, New Jersey).

CCD imaging to detect in vivo luciferase expression. 1.8×10^9 infectious units were injected via tail vein into naive animals or intratumorally. At the specified days, the CCD images were obtained using a cooled IVIS CCD camera (Xenogen, Alameda, California) and images were analyzed[9]. Within the linear range of signal intensity (< saturation limit of 65,000 RLU), we determined that the maximum RLU/min within a region of interest (ROI) to be the most consistent for comparative analysis and that the results correlated closely with luminometry[5,9].

Confocal microscopy and immunohistochemical analysis. Animals were perfused with 2% paraformaldehyde, and lungs were inflated with 3% agarose. In some studies, vessels were visualized by injecting 125 µl of fluorescein-conjugated tomato lectin (Vector Laboratories, Burlingame, California). Specimens were fixed, washed in PBS and embedded on 7% agarose. 500-µm vibrotome sections were stained with a CY-3-conjugated human-specific α-cytokeratin cocktail AM273-5M (BioGenex Laboratories, San Ramon, California). Confocal microscopy (BioRad 1024 confocal microscope; BioRad, Hercules, California) was quantified by ImagePro4.0 software.

Immunohistochemistry was performed on paraffin-embedded tumor sections with antigen retrieval[20]. Tissue sections were incubated at 4° C overnight with respective antibodies, AR-β 5 µg/ml (UpState), or PSA 1:40 (Novocastra, Newcastle upon Tyne, UK). After stringent blocking and washing and incubation with multilink 1:20 (BioGenex) and AP label 1:20 for 20 min at room temperature, sections were washed and developed with DAB (BioGenex).

Effective gene therapy is dependent in part on the ability of a vector to transduce the targeted tissue. We demonstrate that our prostate-specific Ad vector was capable of transducing both the AD LAPC-4 and LAPC-9 (data not shown) xenografts. We also showed that as LAPC-4 tumors progressed from AD to AI, the AI tumor cells continued to express AR and PSA, despite the absence of testicular androgen (Fig. 5). Remarkably, not only was the PSA-based Ad transcriptionally active in AI prostate tumors, it displayed 10-fold higher activity than in AD tumors. As all of the models retain important features of clinical disease[6,7], these data support the possibility that a prostate-targeted vector can be developed to treat patients with advanced disease.

We observed that positive AR staining appeared to be less well localized to the nucleus in the AI than in AD tumor sections (Fig. 4a and data not shown). This observation is consistent with the current understanding that nuclear translocation of AR is mediated in part by androgen binding to the receptor[12]. Both the mechanism of AR translocation and the functional role of nuclear localized AR may be key to understanding transcriptional regulation in AI prostate cancer. Evidence suggests that AR function critical in AI disease includes AR mutations that confer expanded ligand specificity[13], AR over-expression[14], cross-talk between other signaling cascades and AR pathways[15] and increased expression of the nuclear-receptor transcriptional coactivator, TIF2 (ref. 16). In light of mounting evidence supporting an activated AR pathway in AI progression and the fact that PSA transcription is dependent on AR function, the magnitude of serum PSA measured in recurrent disease might not be a good indicator of tumor volume but rather a reflection of AR function. Our vector, composed of PSA-based transcriptional regulatory elements, will provide a tool to interrogate the endogenous AR pathway (Fig. 5c).

One notable, serendipitous discovery was the detection of metastatic lesions. Although the precise transduction mechanism is unclear, we postulated that intratumoral injection of AdPSE-BC-luc leaked to the systemic circulation similar to AdCMV-luc injection and infected the lesions (Fig. 2a). This hypothesis is supported by the fact that lung metastasis can be detected by systemic tail-vein injection of AdPSE-BC-luc (Fig. 4b). An alternative explanation for detecting metastasis after intratumoral vector injection could be the dissemination of a transduced cell(s). This hypothesis is less likely because Ad-mediated expression is transient, and expansion from a single cell to the large lesion would have resulted in loss of expression.

Although several studies have supported the utility of CCD imaging to track the dissemination of luciferase-marked tumor cells in small animals[8], the vector-based approach demonstrated in this study could be developed for future clinical applications. Several areas of refinement are needed. Much higher tissue-specific transcriptional activity, approaching the level of CMV, should increase targeted transduction. We have developed a prostate-specific, two-step transcriptional amplification (TSTA) system that exhibits ~2-fold higher activity than CMV but retains specificity and proper androgen regulation[17]. Approaches

NEW TECHNOLOGY

....

that improve the vectorology (reviewed in ref. 18), such as altering viral transduction to favor specific cell-surface markers, or minimizing viral antigenicity, or use of non-viral vectors could be complementary to the transcriptional targeting approach to further enhance safety and efficacy. The vector-mediated cancer targeting approaches need to be validated in a clinically relevant imaging modality. Positron emission tomography (PET) is a clinical modality that can provide quantitative, three-dimensional localization of imaging signals. In fact, we have demonstrated that micro-positron emission tomography (microPET) can track Ad-mediated herpes simplex virus thymidine kinase gene expression in tumors of living mice[19]. Appropriate resolution of the issues discussed should improve future gene-based prostate cancer diagnostic and therapeutic strategies.

1. Nash, A.F. & Melezinek, I. The role of prostate specific antigen measurement in the detection and management of prostate cancer. *Endocr. Relat. Cancer* **7**, 37–51 (2000).
2. Rini, B.I. & Small, E.J. An update on prostate cancer. *Curr. Opin. Oncol.* **13**, 204–211 (2001).
3. Bloomfield, D.J. *et al.* Economic evaluation of chemotherapy with mitoxantrone plus prednisone for symptomatic hormone-resistant prostate cancer: based on a Canadian randomized trial with palliative end points. *J. Clin. Oncol.* **16**, 2272–2279 (1998).
4. Harrington, K.J., Spitzweg, C., Bateman, A.R., Morris, J.C. & Vile, R.G. Gene therapy for prostate cancer: Current status and future prospects. *J. Urol.* **166**, 1220–1233 (2001).
5. Wu, L. *et al.* Chimeric PSA enhancers exhibit augmented activity in prostate cancer gene therapy vectors. *Gene Ther.* **8**, 1416–1426 (2001).
6. Klein, K.A. *et al.* Progression of metastatic human prostate cancer to androgen independence in immunodeficient SCID mice. *Nature Med.* **3**, 402–408 (1997).
7. Craft, N. *et al.* Evidence for clonal outgrowth of androgen-independent prostate cancer cells from androgen-dependent tumors through a two-step process. *Cancer Res.* **59**, 5030–5036 (1999).
8. Rehemtulla, A. *et al.* Rapid and quantitative assessment of cancer treatment response using *in vivo* bioluminescence imaging. *Neoplasia* **2**, 491–495 (2000).
9. Wu, J.C., Sundaresan, G., Iyer, M. & Gambhir, S.S. Noninvasive optical imaging of firefly luciferase reporter gene expression in skeletal muscles of living mice. *Mol. Ther.* **4**, 297–306 (2001).
10. Tao, N. *et al.* Sequestration of adenoviral vector by Kupffer cells leads to a nonlinear dose response of transduction in liver. *Mol. Ther.* **3**, 28–35 (2001).
11. Yang, Y. *et al.* Cellular immunity to viral antigens limits E1-deleted adenoviruses for gene therapy. *Proc. Natl. Acad. Sci. USA* **91**, 4407–4411 (1994).
12. Waller, A.S., Sharrard, R.M., Berthon, P. & Maitland, N.J. Androgen receptor localisation and turnover in human prostate epithelium treated with the antiandrogen, casodex. *J. Mol. Endocrinol.* **24**, 339–351 (2000).
13. Zhao, X.Y. *et al.* Glucocorticoids can promote androgen-independent growth of prostate cancer cells through a mutated androgen receptor. *Nature Med.* **6**, 703–706 (2000).
14. Linja, M.J. *et al.* Amplification and overexpression of androgen receptor gene in hormone-refractory prostate cancer. *Cancer Res.* **61**, 3550–3555 (2001).
15. Craft, N., Shostak, Y., Carey, M. & Sawyers, C.L. A mechanism for hormone-independent prostate cancer through modulation of androgen receptor signaling by the HER-2/neu tyrosine kinase. *Nature Med.* **5**, 280–285 (1999).
16. Gregory, C.W. *et al.* A mechanism for androgen receptor-mediated prostate cancer recurrence after androgen deprivation therapy. *Cancer Res.* **61**, 4315–4319 (2001).
17. Zhang, L. *et al.* Molecular engineering of a two-step transcription amplification (TSTA) system for transgene delivery in prostate cancer. *Mol. Ther.* **5**, 223–232 (2002).
18. *The Development of Human Gene Therapy.* (ed. Freidmann, T.) (Cold Spring Harbor Laboratory Press, Cold Spring Harbor, New York, 1999).
19. Yaghoubi, S.S. *et al.* Direct correlation between positron emission tomographic images of two reporter genes delivered by two distinct adenoviral vectors. *Gene Ther.* **8**, 1072–1080 (2001).
20. Leav, I. *et al.* Comparative studies of the estrogen receptors β and α and the androgen receptor in normal human prostate glands, dysplasia, and in primary and metastatic carcinoma. *Am. J. Pathol.* **159**, 79–92 (2001).